INL/RPT-22-69181
Revision 0

Synthesis and Thermophysical Property Determination of $NaCl-PuCl_3$ Salts

September 2022

Toni Karlsson[1], Manh-Thuong Nguyen[2], Scott Middlemas[1], Michael Woods[1], Kevin Tolman[1], Vanda Glezakou[3], Ryan Johnson[1], Shawn Reddish[1], Stephen Warmann[1]

[1] *Idaho National Laboratory*
[2] *Pacific Northwest National Laboratory*
[3] *Oak Ridge National Laboratory*

INL Idaho National Laboratory

INL is a U.S. Department of Energy National Laboratory operated by Battelle Energy Alliance, LLC

INL/RPT-22-69181
Revision 0

Synthesis and Thermophysical Property Determination of NaCl-$PuCl_3$ Salts

Toni Karlsson, Manh-Thuong Nguyen, Scott Middlemas, Michael Woods, Kevin Tolman, Vanda Glezakou, Ryan Johnson, Shawn Reddish, Stephen Warmann

September 2022

Idaho National Laboratory
Advanced Reactor Technologies
Pyrochemistry & Molten Salts Systems Group, C420
Idaho Falls, Idaho 83415

Prepared for the
U.S. Department of Energy
Under DOE Idaho Operations Office
Contract DE-AC07-05ID14517

Page intentionally left blank

INL ART Program

Synthesis and Thermophysical Property Determination of $NaCl\text{-}PuCl_3$ Salts

INL/RPT-22-69181
Revision 0

September 2022

Technical Reviewer: (Confirmation of mathematical accuracy, and correctness of data and appropriateness of assumptions.)

Guy Fredrickson — 9/13/2022

Guy Fredrickson — Date

Approved by:

M. Davenport — 9/13/2022

Michael E. Davenport — Date
ART Project Manager

Travis Mitchell — 9/13/2022

Travis R. Mitchell — Date
ART Program Manager

Michelle Sharp — 9/13/2022

Michelle T. Sharp — Date
INL Quality Assurance

ABSTRACT

Currently, a knowledge gap exists in the available data and understanding of thermophysical properties relating to fresh fuel salts, especially those containing plutonium. This data is necessary for the design and construction of test reactors, as well as the licensing of future commercial molten-salt reactors. Thermophysical properties such as melting temperature, salt stability, density, and heat capacity were determined using synthesized eutectic NaCl-$PuCl_3$ (36 mol% $PuCl_3$) and a more sodium rich composition containing 25 mol% $PuCl_3$. These measurements document the baseline properties of the salt as a function of temperature for future experiments on irradiated fuel salt which will provide a holistic perspective on the change of thermophysical properties during reactor operations. It was determined that the NaCl-$PuCl_3$ ingot synthesized for this study contained 63.4 mol% NaCl, 36.3 mol% $PuCl_3$ and was 99.7% pure. Upon heating the NaCl-$PuCl_3$ eutectic was stable at temperatures up to 800°C. The onset of melting occurred at 451°C, and the enthalpy of fusion was determined to be 140.7 ± 8.4 J/g. Specific heat capacity measurements showed a slightly decreasing trend with respect to temperature in the liquid phase ranging from 0.67 to 0.57 J/g·K, with an average value of 0.637 ± 0.03 J/g·K (104 ± 5 J/mol·K) between 500 to 720°C. Three independent trials of the molten NaCl-$PuCl_3$ eutectic salt found the density to be $\rho(T) = 3.8589 - 9.5342 \cdot 10^{-4}\ T(°C)$, validated between 500 to 800°C. In addition to salt synthesis and experimentally determining thermodynamic properties, ab initio molecular dynamic (AIMD) simulations were used to calculate density and heat capacity values.

ACKNOWLEDGEMENTS

The team would like to acknowledge the facilities at the Idaho National Laboratory (INL) for supporting this research. This work was supported by multiple projects. The salt synthesis work was supported under CRADA 21CRA25 “Flowing Molten Salt Microloop Testing Using Actinide Bearing Salts” in collaboration with TerraPower, LLC. Elemental and isotopic analysis and the majority of the thermophysical property research was supported by the Molten Salt Reactor Campaign, work package number AT-22IN070502 “Thermochemical and Thermophysical Property Database Development – INL.” Finally, density measurements were, in part, supported through the INL Laboratory Directed Research and Development Program under Department of Energy’s Idaho Operations Office Contract DE-AC07-05ID14517.

Page intentionally left blank

CONTENTS

FIGURES

TABLES

Page intentionally left blank

ACRONYMS

AFCI	Advanced Fuel Cycle Initiative
AIMD	Ab Initio Molecular Dynamics
ASTM	American Standard Test Method
CMD	Classical force field molecular dynamics
DSC	Differential Scanning Calorimeter
ICDD	International Centre for Diffraction Database
ICP OES	Inductively Coupled Plasma Optical Emission Spectroscopy
INL	Idaho National Laboratory
MSR	Molten-Salt Reactors
NIST	National Institute of Standards and Technology
NPT	number of particles, pressure, and temperature are conserved
NVT	number of particles, volume, and temperature are conserved
Q-ICP-MS	Quadrupole - Inductively Coupled Plasma - Mass Spectrometry
STA	Simultaneous Thermal Analyzer
TGA	Thermogravimetric Analyzer
UTEVA	Uranium and Tetra Valent Actinides
XRD	X-ray Diffraction

Page intentionally left blank

1. INTRODUCTION

The use of sodium chloride (NaCl) - plutonium trichloride ($PuCl_3$) as a fuel in molten-salt reactors (MSR) has been discussed for decades [1-3]. Today, society's rapid shift toward renewable energies and push for carbon neutral energy sources to mitigate climate change have renewed interest in using nuclear energy as a low-carbon footprint energy source [4]. Advanced MSRs are one potential type of nuclear reactor design being considered today by several countries including the United States, Canada, China, South Korea, Norway, and Denmark. Fuel compositions of actinide fluoride and chlorides are typically considered; however, a recent study on heavier halides indicates that bromide and iodine fuels may also be possible [5]. A limited amount of experimental thermophysical property data is available on the NaCl-$PuCl_3$ fuel salt system; furthermore, most information available relates to the unary actinide salts or mixtures which have been theoretically calculated and remain unverified experimentally.

Some of the challenges that arise when studying systems containing $PuCl_3$ are the availability of a pure $PuCl_3$ feedstock and facilities with characterization equipment that allows the use of transuranic materials. Synthesis of high-purity $PuCl_3$ has been demonstrated, at the gram scale, by aqueous, gaseous, and electrochemical methods [6-8]. There are several documented chemical reactions for producing $PuCl_3$, each using a different precursor. $PuCl_3$ can be synthesized from the reaction of PuO_2 or plutonium (III) oxalate with PCl_5, SCl_2, HCl-H_2, $COCl_2$, and CCl_4. However, these are either not scalable reactions or do not yield a $PuCl_3$ product >98% pure [6] except with $COCl_2$ [9]. Aqueous preparation of $PuCl_3$ can be complicated by difficulties associated with obtaining a pure solution of Pu(III) and removing all water of crystallization; however, 98% pure $PuCl_3$ has been achieved [10]. Therefore, synthesis and purification of $PuCl_3$ are typically achieved through high-temperature pyrochemical processing where the PuO_2 feedstock is converted to Pu metal by direct reduction in $CaCl_2$ through the multicycle direct oxide reduction process [11]. However, if complete chlorination of Pu is not ensured, it can have unintended effects on thermophysical properties, especially melting temperature [12].

A lesser utilized synthesis route is proposed in this research, where NH_4Cl is used as the chlorinating agent at elevated temperatures and has been shown to yield a high-purity UCl_3 product [13]. The overall reaction is represented in Reaction 1. NH_4Cl sublimates at 338°C [14] represented by Reaction 2, and its decomposition is therefore the source of HCl gas. Reaction of Pu metal with HCl gas is highly exothermic, Reaction 3, and because this route of chlorination is a solid-gas reaction, the Pu metal must be pulverized to increase the surface area and ensure complete chlorination. Extreme care should be taken when handling Pu-metal powders which are pyrophoric and must be handled in an inert atmosphere. Because the Pu-Cl reaction is highly exothermic, an inert carrier salt, such as NaCl, can be added to the reaction vessel to absorb some of the energy produced during the chlorination. The complete synthesis reaction follows Reaction 4, where the intended product was the eutectic NaCl-$PuCl_3$ binary containing 36 mol% $PuCl_3$ reported by Bjorklund et al. [15], and NaCl is present as both a product and reactant. Gibbs free energy calculations were performed by HSC Software [16].

$$Pu + 3NH_4Cl \rightarrow PuCl_3 + 3NH_3 + 1.5H_2 \quad \Delta G_{Rx,338°C} = -505\ kJ \qquad \text{Reaction 1}$$

$$NH_4Cl(s) \rightarrow NH_3(g) + HCl(g) \quad \Delta G_{Rx,338°C} = -505\ kJ \qquad \text{Reaction 2}$$

$$Pu(s) + 3HCl(g) \rightarrow PuCl_3(s) + 1.5H_2(g) \quad \Delta G_{Rx,338°C} = -527kJ \qquad \text{Reaction 3}$$

$$Pu + NH_4Cl + NaCl \rightarrow PuCl_3 + NaCl + NH_3 + H_2 \qquad \text{Reaction 4}$$

One issue that currently inhibits development and deploying advanced MSRs is a lack of understanding of molten-salt behavior and molten-salt thermophysical property changes due to impurities, such as those arising from salt fabrication, handling (i.e., oxygen and moisture), and corrosion. Therefore, it is necessary to understand the fundamental behaviors such as melting and polymorphic temperatures, heat capacity, and density of actinide-bearing salts proposed for use as fuels in MSRs. This type of data along with other information such as corrosion kinetics will aid in modeling and simulation.

Thermophysical properties of NaCl are well known. However, limited data is present in literature on the unary $PuCl_3$ salt and even less information is available for mixtures of NaCl and $PuCl_3$. Thermophysical properties for NaCl and $PuCl_3$ are provided in Table 1. In this work, eutectic NaCl-$PuCl_3$ (64 mol% NaCl – 36 mol% PuCl3) was synthesized along with 75 mol% NaCl - 25 mol% $PuCl_3$ salt. Both were characterized to provide a better understanding of NaCl-$PuCl_3$ mixtures melting temperature, salt stability, density, and heat capacity in the temperature range or an operating MSR. In addition, experimental data for density and heat capacity are compared to computational values determined by ab initio molecular dynamic (AIMD) simulations to provide further insights on the similarities and contrasts existing in both approaches.

Table 1. Properties of NaCl and $PuCl_3$ in their crystalline form.

Property	NaCl (cr)	Ref.	$PuCl_3$ (cr)	Ref.
Appearance	Clear to white	[17]	Green-blue	[18]
Melting Temperature, °C	801	[17]	736 ± 10 760 767 ± 2 760 to 765 768	[19] [10] [15] [20] [21]
Boiling Temperature, °C	1413	[17]	1679 1730	[19] [5]
Density (solid), g/cm^3	2.165	[17]	5.708	[22]
Specific Heat (J/mol·K)	50.33	[23]	101.2	[5, 22]
Heat of Fusion, kJ/mol	517	[17]	55.0 ± 5.0 63.6	[24] [25]

2. METHODS

All material handling and experimentation were performed in an inert atmosphere glovebox with oxygen and moisture levels maintained below 5 and 0.1 ppm, respectively. Physical measurements of all masses were measured using a calibrated analytical balance. Balances are calibrated annually by the standards and calibration laboratory (S&CL) at the Idaho National Laboratory (INL), and they are assigned an uncertainty for their measurement range. Daily checks are performed on these balances using National Institute of Standards and Technology (NIST) traceable external calibration weights, also calibrated by the S&CL, to confirm the balance functionality and accuracy before use.

2.1 Salt Synthesis

Prior to use, sodium chloride (NaCl, 99.99% metals basis) was heated under a 17.5 kPa absolute vacuum to 350°C for 3.5 hours in an argon glovebox to ensure it was fully dry before being transferred and weighed in the Advanced Fuel Cycle Initiative (AFCI) Glovebox at INL. Ammonium chloride

(NH_4Cl, 99.99%) was heated to 100°C and held for 8 hours. The particle size of NaCl and NH_4Cl was reduced using an agate mortar and pestle to less than 50 mesh. Plutonium metal, in rodlet form, was selected as the feedstock material because of its purity and ease of size reduction. Visually, the Pu-metal rod appeared to be free from surface oxidation (Figure 1A). All labware in contact with materials during synthesis and experimentation was cleaned with soapy water, rinsed in deionized water, dried with ethanol, rinsed with deionized water, dried in an oven, and then heated to temperature prior to use in a furnace.

Prior to hydriding the Pu-metal rods (Figure 1A), further size reduction was performed using sheers to cut segments into small pellets approximately 3–5 mm in diameter as seen in Figure 1B. To increase the surface available for reaction, the Pu-metal pellets were exposed to hydrogen gas at elevated temperatures. Exposure of Pu metal to hydrogen gas leads to the formation of PuH_x where the stoichiometry is dependent on temperature and pressure [26]. The reaction for hydriding follows Reaction 5; this reaction will proceed at a rapid rate, independent of temperature but dependent on the hydrogen partial pressure and active surface area [27].

$$Pu + \frac{x}{2}H_2 \rightleftharpoons PuH_x \qquad \text{Reaction 5}$$

The furnace hydriding furnace was prepared by placing the Pu-metal sample in a tapered quartz crucible (4.5 cm inner diameter at base), evacuating the furnace chamber to approximately 3.07 kPa, and backfilling with a flowing hydrogen purge gas (H_2, 99.99%) at a rate of 20 standard cubic centimeter per minute. The furnace was then heated to 250°C and held for 60 minutes with the H_2 purge. After the 60 minutes, the furnace was cooled to room temperature, evacuated, and reheated to 250°C with a H_2 purge. This heating, cooling, and evacuation cycle was repeated five times in an attempt to dislodge the hydride material from the Pu-metal pellets, exposing more metal surface for reaction with H_2 gas. The material was removed from the furnace and sieved. Material <50 mesh was held to the side while material >50 mesh went through the hydride process until all material was below 50 mesh (Figure 1C). To de-hydride, a final step was performed where the material was heated to 325°C under vacuum and held for several hours. No hydrogen analysis was performed on the material to confirm completeness as the presence of some PuH_2 is not detrimental to the chlorination step due to the high favorable thermodynamic chlorination reaction.

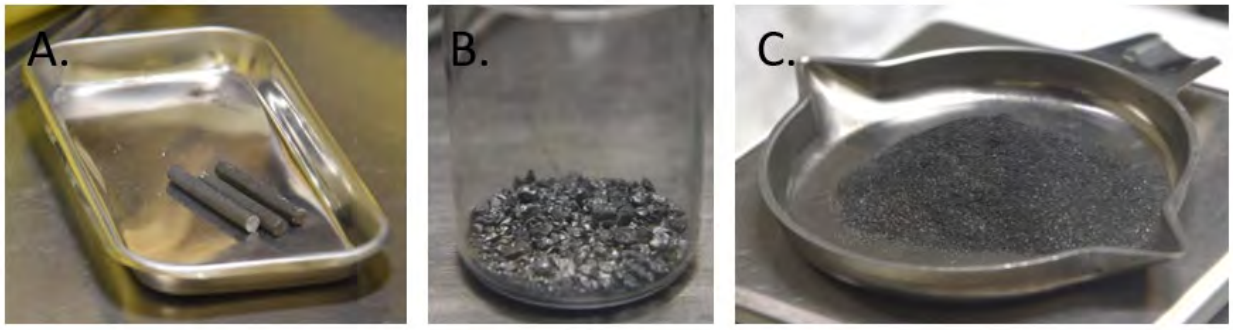

Figure 1. Plutonium metal. A. metal rods, B. intermediate particles, C. less than 50 mesh powder.

The Pu-powder was chlorinated using NH_4Cl which is an exothermic reaction; to absorb some of the energy, sodium chloride was added to the mixture as a "heat sink." In addition, the eutectic NaCl-$PuCl_3$ was the desired product so adding NaCl to the reaction container eliminated a further blending step.

Two batches of Pu metal were size reduced using the hydride, de-hydride process, approximately 150.0g each. Two batches of NaCl-$PuCl_3$ eutectic salt were synthesized, approximately 250g in mass each. First, the NaCl and NH_4Cl were mixed, with NH_4Cl added in 2% excess. Excess chlorine gas causing the formation of $PuCl_4$ was not of concern as $PuCl_4$ has been shown, by calculations, to not exist

in the solid state but to exist in the gaseous state in an atmosphere of chlorine over $PuCl_3$ [28]. Though $PuCl_4$ has not been isolated in the solid or gaseous state, its presence has been inferred due to increased volatility of $PuCl_3$ in a stream of chlorine at 400°C relative to H-HCl stream. However, it is thought that gaseous $PuCl_4$ decomposes back to $PuCl_3$ and chlorine gas when condensed. This is in contrast to UCl_3 which has been shown to form volatile UCl_4 when in the presence of excess chlorine [29].

Pu-metal powder was added to the NaCl-NH_4Cl mixture in a glass jar (Figure 2A) and then lightly mixed into a homogenous blend as seen in Figure 2B. Finally, the homogenous mixture was poured into a glassy carbon crucible (Sigradur, GAT 32, 320 ml) shown in Figure 2C and placed into a modified benchtop furnace (Kerr, Auto Electro-Melt Furnace, Maxi 3 kg). A glassy carbon cover (Sidradur GAD 3) was placed on the crucible. Steel wool was placed on top of the crucible lid to react with any chlorine gas should it escape the reaction vessel. This was all contained within the furnace which included an insulated lid. The synthesis reaction vessel and furnace were located within the argon atmosphere AFCI glovebox. During synthesis, ammonia and HCl gas detectors (Dräger diffusion tubes) were placed on top of the furnace and at various location in the glovebox.

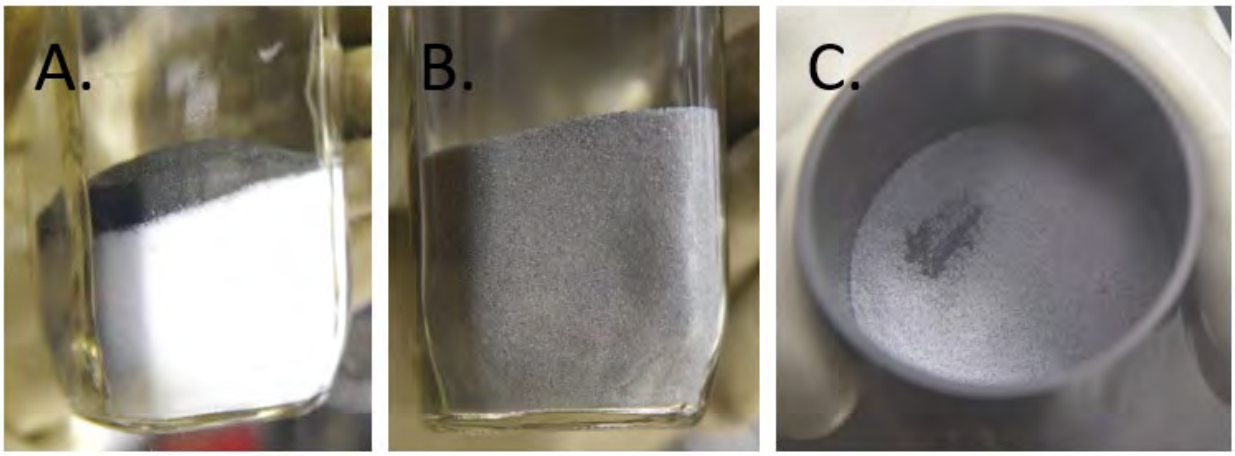

Figure 2. Homogenization of chemicals for synthesis of eutectic NaCl-$PuCl_3$ salt. A. Unmixed NaCl, NH_4Cl, and Pu-metal powders; B. Mixed chemicals in glass vial; C. Mixed material in glassy carbon crucible, reaction vessel.

Because the Pu-chlorination reaction is exothermic and has the potential to instantaneously release a large amount of energy, the synthesis reaction was performed over approximately a 60-hour period. Time zero began at room temperature, and the furnace was heated to 450°C with a heating rate of 10°C/hour. The critical temperature for the reaction was thought to be 338°C, the sublimation temperature of NH_4Cl. However, NH_3 gas was detected when the furnace reached 175°C, suggesting the chlorination reaction initiated at lower temperatures than expected. Once the furnace reached 450°C, the material was heated at 5°C/min to 800°C and then cooled to room temperature. Once cool, the NaCl-$PuCl_3$ ingot was easily removed from the glassy carbon crucible. No discoloration was seen on the steel wool, the crucible lid, or the walls of the crucible that would indicate volatility of the NaCl-$PuCl_3$ product.

2.2 Elemental and Isotopic Analysis

Both the Pu-metal powder and the resulting NaCl-$PuCl_3$ salt samples were dissolved in a solution containing several strong inorganic acids to ensure the sample and any metal impurities would be dissolved. Before trace analysis of impurities could be carried out by inductively coupled optical emissions spectrometry (ICP OES), a portion of the parent solution was chemically separated to remove the plutonium from the matrix. Plutonium has a rich emission spectrum which can interfere with

determining other analytes of interest, particularly if they are present in only trace quantities. The separations were carried out using auto-gas-pressurized extraction chromatography (auto-GPEC). Once the sample is loaded into the auto-GPEC, a valve switches/rotates, opening to a pressurized-gas line, and the sample is then pushed through the chromatographic column, and the eluent is collected on the other side. To remove the plutonium, a uranium and tetra valent actinides (UTEVA, Eichrom) 100–150 μm resin was employed as the stationary phase. The removal of the plutonium is required before the ICP-OES analysis because emission from plutonium can interfere with determining other elements of interest, specifically iron. Isotopic analysis was performed on the quadrupole – inductively coupled plasma - mass spectrometer (Q-ICP-MS) which does not require separation prior to analysis, and therefore, a portion of the parent solution was simply diluted to prepare it for analysis.

Crystallographic X-ray diffraction (XRD) data were acquired on a Panalytical Empyrean X-ray diffractometer (Malvern-Panalytical Ltd United Kingdom) operating with a Bragg-Brentano geometry monochromatic Cu-K_α beam radiation (λ=1.540593 Å). The salt sample(s) were analyzed by adjusting the voltage and current values to 40-kV and 45-mA, respectively, and rotating the sample(s) on the diffractometer reflection sample holder spinner at a rotational speed of 15 rpm. Scanning was conducted from 10° to 70° 2θ with a 0.026-degree step size interval. A NIST LaB6 standard (SRM 660c) was used to determine instrument parameters and verify instrument alignment. The background was fitted with a Sonneveld & Visser polynomial [30] with a zero bending factor and eight granularity to fit the background. Rietveld fits to the data were conducted using a computer software program (HighScore Plus; Malvern-Panalytical) and using International Centre for Diffraction Database (ICDD) PDF4+. Refinements for plutonium trichloride were conducted in hexagonal space group P63/m (No.176) using ICDD reference 00-006-0222 and for sodium chloride in cubic space group Fm-3m (No.225) using ICDD reference 00-002-818.

2.3 Melting Temperature, Salt Stability, and Enthalpy

Transition temperatures and enthalpies of transition were determined employing a simultaneous thermal analyzer (STA), Netzsch 449 F1, with differential scanning calorimeter (DSC)/thermogravimetric analyzer (TGA) type-S sample carrier, located inside an inert argon glovebox having oxygen and moisture levels below 5 ppm and 0.1 ppm, respectively. Inert, glassy carbon crucibles (diameter 6 mm, 50 μl) and lids, rated to 2400°C, were used to contain the salt samples and calibration standards. Crucible lids contained a small hole in the center to prevent a buildup of pressure in the crucible and allow the escape of off gasses (if they were to occur).

Calibration of the STA for temperature and heat flow was performed using five high-purity standards for each of the three heating rates: 20, 10, 2°C/min. The transition temperatures and enthalpy of the standards were calculated by averaging the onset and peak area for three heating cycles [31]. Enthalpies of transition were determined by integrating the full area under each transition peak from the transition start to the transition finish. The temperature and sensitivity calibrations were accurate in the range of 164 to 962°C by verification using a zinc standard (Table 2) where the experimental melting temperature was within ±3°C and < ±1°C with a heating rate of 20 and 2°C/min, respectively. The enthalpy of zinc at different heating rates was accurate to ±3%.

Table 2. Experimental STA results of zinc run using the temperature and heat flow calibration files at multiple heating rates.

Heating Rate	Cycle 1	Cycle 2	Cycle 3	Average	Deviation	Error
°C/min	°C	°C	°C	°C	°C	%
20	417.0	416.9	416.9	416.9	2.6	-0.61
10	418.4	418.2	418.2	418.3	1.2	-0.29
2	419.1	419.0	419.0	419.0	0.5	-0.11
°C/min	J/g	J/g	J/g	J/g	J/g	%
20	105.5	105.4	104.9	105.3	2.2	-2.08
10	108.3	108.0	107.8	108.0	-0.5	0.50
2	104.8	104.4	103.9	104.4	3.1	-2.91

The reported eutectic and melting point temperatures were determined using the average of the onset temperature or ending peak temperature for melting, derived from the heating segment of three separate heating and cooling cycles. The reported onset and melting temperatures were determined using linear regression to remove the effects of thermal lag from the samples. All temperatures are reported with an accuracy of < ± 5°C [32].

The stability of the salts was studied by monitoring the mass change as a function of temperature. A correction file was generated, prior to sample analysis, using two empty crucibles (i.e., sample and reference) with identical heating conditions under which the sample was run to account for artificial changes in mass due to buoyancy effects. Once the correction was generated, the sample was loaded into the same sample crucible used in the correction file.

2.4 Heat Capacity

Specific heat capacity measurements were conducted using a Netzsch 404 F1 DSC with a type-S sample carrier and rhodium furnace. Prior to heat capacity measurements, the DSC was calibrated for temperature and heat flow as described previously for the STA. A heating rate of 5°C/min was used for all calibration standards and during specific heat capacity measurements. The accuracy of the temperature and sensitivity calibration was verified using one or more standards and performed according to ASTM E967-18 [31]. Verification of the calibration curves showed that the DSC was calibrated to have deviation in experimental melting temperature from theoretical values of < ±1°C, and the heat flow was calibrated to be < 2% for aluminum.

Heat capacity was determined using the C_p ratio method where the measurement consisted of several experimental runs including baseline (empty crucible, no sample), standard + baseline (sapphire with same crucibles as baseline), and sample + baseline (same crucible as baseline and standard). When determining heat capacity, a new sensitivity calibration file may be generated from the sapphire standard. However, the sensitivity calibration generated using the high-purity standards may also be used depending on which one provides the most accurate heat capacity for sapphire within the temperature range of interest. Specific heat as a function of temperature at constant pressure was calculated by Equation 1 and requires three measurements be taken under the same experimental conditions.

$$C_p = \frac{m_{Standard}}{m_{Sample}} \cdot \frac{DSC_{Sample} - DSC_{Baseline}}{DSC_{Standard} - DSC_{Baseline}} \cdot C_{p_{Standard}} \quad \text{Equation 1}$$

Measurement of heat capacity involved nine separate measurements using the same sample and reference crucible. First, three baseline correction measurements were performed. The first was discarded, and the second and third baseline correction were used to verify reproducibility. Next, three measurements were run using a NIST sapphire standard with the selected baseline. The first sapphire run was used to generate a sapphire heat flow calibration, replacing the heat flow calibration generated using the standards. The second and third sapphire runs were used to verify that the measured specific heat capacity of sapphire matched the values for theoretical sapphire heat capacity. Finally, the salt sample was loaded into the crucible and run three times using the same baseline as the sapphire sample. The average heat capacity of the three sample measurements is reported as the heat capacity for that sample. Specific heat capacity determination was performed in accordance with American Standard Test Method (ASTM) standard procedure [33].

2.5 Density

For the NaCl-$PuCl_3$ eutectic density determination, 35.250g of salt was added to a glassy carbon crucible previously cleaned with deionized water and isopropyl alcohol and baked in a furnace at 800°C for 2 hours. The glassy carbon crucible containing the salt sample was then placed in a benchtop furnace (Kerr, Auto Electro-Melt Furnace, Maxi 3 kg) modified for density experiments. Figure 3 shows the Archimedes densitometer setup within the glovebox including the furnace, stand, and bottom hanging balance and is described in greater detail by Duemmler et al. [34]. A Ni bobber was tied onto the wire and its volume calculated in 10 mL of both deionized water and ethanol, which have well defined densities near room temperature. The average of these calculations gave a volume of 1.0408 ± 0.0006 cm^3. The mass of the bobber and wire was then measured in argon using the hang down balance (Mettler Toledo WXSS204, tolerance 0.8 mg). The crucible with salts, quartz lid, and bobber with wire were added to the setup and the salt melted. Once eutectic NaCl-$PuCl_3$ measurements were completed, an addition of 5.60g of NaCl was added to eutectic salt in the crucible to achieve a 25mol% $PuCl_3$ in NaCl composition and the density of this mixture was determined.

Figure 3. Experimental density setup showing bottom-loading balance on the stand above a furnace with quartz lid and thermocouple inserted inside the AFCI glovebox.

Mass readings were performed after 5 minutes of thermal stability at each temperature as measured by an Inconel-sheathed K-type thermocouple (OMEGA) inserted directly into the salts. This equilibration was on average 60 minutes after each temperature change of approximately 50°C. An internal adjustment of the balance was performed before each set of mass measurements at a unique temperature. The balance was tared before each measurement. Density measurements were first taken at increasing temperature intervals between 525 and 800°C and then with decreasing temperatures between 800 to 525°C and finally a randomized temperature schedule.

The density calculations were performed using the direct Archimedean method based on measurement of buoyancy force exerted on a bobber submerged in molten salts. The density of the salt at an experimental temperature is calculated by Equation 2 where m_{argon} is the measured mass of the bobber and wire suspended in argon, w_{salts} is the measured weight of the bobber and wire suspended in the salts, g is the acceleration due to the gravity of Earth, α is the linear thermal coefficient of expansion of nickel, T is the salt temperature, and T_0 is the reference temperature for V_0, the reference volume of the nickel bobber. The linear thermal coefficient of expansion of nickel was calculated based on a polynomial fit of reference data [35].

$$\rho_{salts} = \frac{m_{argon} - w_{salts}}{V_0(1+3\alpha(T-T_0))} \quad \text{Equation 2}$$

The experimental uncertainty of the density was calculated by the propagation of individual uncertainties. Equation 3 shows the fundamental form of the uncertainty propagation of Equation 2. Equation 4 shows the simplified experimental uncertainty function, and Table 3 lists the individual uncertainties and their explanations.

$$\sigma_{\rho_{salt}}^2 = \left(\frac{\partial \rho_{salt}}{\partial m_{argon}}\right)^2 \sigma_{m_{argon}}^2 + \left(\frac{\partial \rho_{salt}}{\partial w_{salt}}\right)^2 \sigma_{w_{salt}}^2 + \left(\frac{\partial \rho_{salt}}{\partial V_0}\right)^2 \sigma_{V_0}^2 + \left(\frac{\partial \rho_{salt}}{\partial \alpha}\right)^2 \sigma_{\alpha}^2 + \left(\frac{\partial \rho_{salt}}{\partial T}\right)^2 \sigma_T^2 \quad \text{Equation 3}$$

$$\sigma_{\rho_{salt}} = \rho_{salt} \sqrt{\frac{\sigma_{m_{argon}}^2 + \sigma_{w_{salt}}^2}{(m_{argon} - w_{salt})^2} + \frac{\sigma_{V_0}^2}{V_0^2} + \frac{9\alpha^2(T-T_0)^2}{(1+3\alpha(T-T_0))^2}\left(\frac{\sigma_\alpha^2}{\alpha^2} + \frac{\sigma_T^2}{(T-T_0)^2}\right)} \quad \text{Equation 4}$$

Table 3. Definition of terms used to calculate the error associated with liquid density measurements.

Symbol	Explanation
$\sigma_{m_{argon}}$	Standard deviation of the five weight measurements in argon
$\sigma_{w_{salt}}$	Standard deviation of the five weight measurements in salt
σ_{V_0}	Standard deviation of the two calculated volumes from water and ethanol benchtop trial
σ_α	Assigned as 1% of value of α
σ_T	OMEGA assigned 0.05% * T + 0.3°C

2.6 Computation

Since research on transuranic salts is sparce in literature, timely, expensive, and hazardous, AIMD simulations were used to investigate two NaCl-$PuCl_3$ salt compositions at different temperatures; a

summary of compositions is provided in Table 4. Comparing experimental and calculated, density and heat capacity results, will aid in refining the modeled data and yield more accurate models.

All simulations were conducted using the CP2K package [36, 37]. Classical force field molecular dynamics (CMD) were used initially to relax the system and provide starting configurations for the AIMD simulations. For CMD, the polarized ionic model (PIM) [38] was used to represent interatomic interactions. The density of the system was optimized within the "number of particles, pressure, and temperature are conserved" (NPT) ensemble, where the pressure and temperature were maintained with the Parrinello-Raman barostats [39] and Nose-Hoover thermostat [40], respectively.

The AIMD simulations were performed with the Perdew-Burke-Ernzerhof density functional [41] including Grimme's D3 van der Waals corrections [42] with the Goedecker-Teter-Hutter pseudopotentials [43, 44]. The double zeta valence polarized [44-46] Gaussian basis functions were used for the valance states of Pu($6s^2\ 6p^6\ 5f^6\ 7s^2$), Na($2s^2\ 2p^6\ 3s^1$), and Cl($3s^2\ 3p^5$) with a plane wave cutoff of 900 Ry in conjunction with the Gaussian plane wave hybrid basis set framework [47]. Molecular dynamics simulations were conducted within both the NPT and "number of particles, volume, and temperature are conserved" (NVT) ensembles. In NPT simulations, the pressure and temperature were maintained with the Parrinello-Raman barostats [39] and Nose-Hoover thermostat [40], respectively.

Table 4. Compositions and temperatures used in simulations.

	16 mol% $PuCl_3$	25 mol% $PuCl_3$	36 mol% $PuCl_3$
Number of Cl atoms	66	78	86
Number of Pu atoms	8	13	18
Number of Na atoms	42	39	32
Temperatures (K)	1000, 1257	898, 973, 1073	730, 900, 1100

3. RESULTS

Two separate salt syntheses were performed. Both yielding an approximate 250g NaCl-$PuCl_3$ ingot close to the eutectic composition of 64 mol% NaCl – 36 mol% $PuCl_3$. Each ingot was easily released from the glassy carbon crucible and appeared to be black with a teal hue in color (Figure 4A). After size reduction, the powdered material was blue green in color (Figure 4B)—closely matching the color reported for $PuCl_3$ [18].

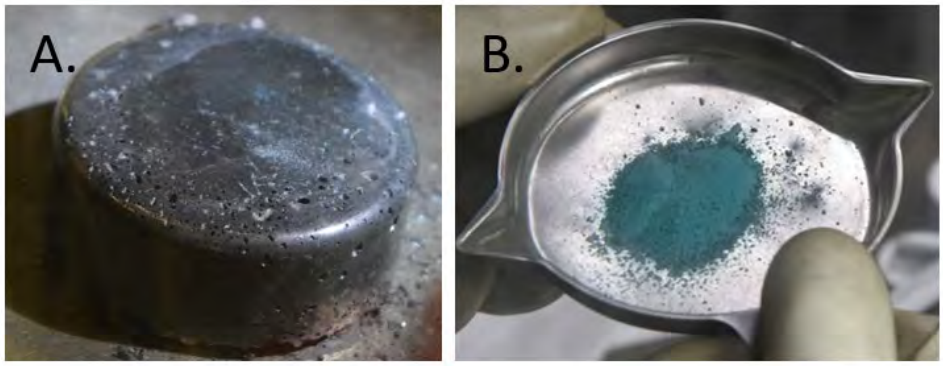

Figure 4. NaCl-$PuCl_3$ eutectic material; A. solid ingot form, B. powder form.

3.1 Elemental and Isotopic Analysis

Elemental and isotopic results from Q-ICP-MS, ICP-OES, and gamma spectroscopy for the Pu-metal and synthesized NaCl-$PuCl_3$ ingot are provided in Table 5. Elements which were below the detection limit

of each instrument are not listed in Table 5. It can be concluded from the elemental and isotopic analysis of the salt that there are no major impurities in the Pu-metal with the exception of a small amount of iron, as well as uranium, and americium present as decay products.

Table 5. Elemental and isotopic composition of the Pu-metal starting and the synthesized NaCl-$PuCl_3$ ingot.

Q-ICP-MS	Pu-metal		NaCl-$PuCl_3$ salt	
Analyte	ug/g	% Error	ug/g	% Error
U-234	118	±10%	60.4	±10%
U-235	792	±5%	406	±5%
U-236	556	±5%	283	±5%
m/z -238	430	±5%	246	±5%
Np-237	390	±5%	212	±5%
Pu-239	807000	±5%	469000	±5%
Pu-240	157000	±5%	91600	±5%
m/z-241	10100	±5%	6040	±5%
m/z-242	3350	±5%	1960	±5%
Sr-88	<40	N/A	8.06	±15%
Ag-109	10.7	±20%	11.7	±20%
Ba-138	<30	N/A	11.7	±15%
ICP-OES				
Analyte	ug/g	% Error	ug/g	% Error
Fe	91.0	± 25 %	72.7	± 30 %
Na	<320	N/A	94900	±5%
Pr	<30	N/A	83.8	± 20 %
Gamma Spectroscopy				
Species	uCi/g	% Error	uCi/g	% Error
Am-241*	25100	±3%	14100	±3%
* The specific activity of Am-241 is 3.428 Ci/g [48].				

Analysis results of the ICP-OES, Q-ICP-MS and gamma spectroscopy data are provided in Table 6. Mass balance suggests there was a 106% recovery of the sample but within the expected error. The quantities of Am-241 and Pu-241 were determined by subtracting the Am-241 concentration (gamma spectroscopy) from the total m/x-241 value (Q-ICP-MS). NaCl and $PuCl_3$ values indicate that the fabricated NaCl-$PuCl_3$ ingot contains 63.4 mol% NaCl and 36.3 mol% $PuCl_3$. The experimentally reported eutectic composition contains 36 mol% $PuCl_3$ [15]; therefore, the salt fabricated for this study is very nearly the reported eutectic composition. Other studies calculate the eutectic composition of $PuCl_3$ to be 38.3 mol% [49] or 37.4 mol% [50]. Impurities and compounds other than NaCl and $PuCl_3$ account for < 0.32 mol% of the ingot. The concentrations of Sr-88, Ag-109, Ba-137, Fe, and Pr are not accounted for since they are < 0.03% of the total sample. It was therefore determined by elemental and isotopic evaluation that the NaCl-$PuCl_3$ ingot material synthesized had a purity of 99.7%.

Table 6. Composition of the NaCl-$PuCl_3$ ingot by conversion to chlorides assumed NaCl and formation of Pu, U, Np, and Am to their respective trichloride.

Element	Metal	Metal Chloride	wt. %	mol %
	g/g	g/g		
Na	0.0949	0.2412	22.66	63.41
Total U	0.0007	0.0011	0.10	0.05
Total Pu	0.5647	0.8159	76.65	36.27
Np	0.0002	0.0003	0.03	0.01
Am	0.0041	0.0059	0.56	0.26
Total	0.6647	1.0644	100.00	100.00

A XRD pattern of 84 mg NaCl-$PuCl_3$ powder was analyzed for phase purity. This sample was hygroscopic and needed an inert atmosphere during XRD. The sample was loaded into a gas-tight-dome holder to keep argon gas atmosphere around this sample during the data collection inside the diffractometer. The black tick marks in Figure 5 represents the combined reported lines used to fit this pattern for $PuCl_3$ hexagonal space group P63/m (No.176) using ICDD reference 00-006-0222 and NaCl cubic space group Fm-3m (No.225) using ICDD reference 00-002-818. The blue curve is the collected diffraction data for this sample with identified peaks for $PuCl_3$ and NaCl. These peaks are identified with their respective phases and indicated by green and red dots above the identified peaks. The XRD holder is equipped with a polymer dome on this gas-tight sample holder and resulted in amorphous x-ray scatter and can be seen in the XRD data as the hump between 10 to 25° 2-theta. There were some additional peaks that could be seen in the data and are likely from a monoclinic phase, which could indicate the presence of an oxy-chloride phase. Several XRD patterns were collected over a 2-day period, as time passed peaks 15 and 16°, 2-theta became more visible suggesting that air was contaminating the sample over time. The peak shown in Figure 5 was collected less than 1 hour after removing the sample from the glovebox.

The lattice dimensions, for PuCl3 determined by x-ray diffraction are $a_1 = 7.380 \pm 0.001$ Å and $a_3 = 4.238 \pm 0.001$ Å [51]. The refined structure for eutectic NaCl-$PuCl_3$ showed lattice dimensions of $a_1 = 7.506$Å and $a_3 = 4.237$Å. The lattice constants obtained in this work show that the eutectic NaCl-$PuCl_3$ composition has an increase lattice constant for a_1 of 0.126Å, while the a_3 remained unchanged from $PuCl_3$ reported values in literature. Similar behavior was exhibited in the eutectic NaCl-UCl_3 system when compared to UCl_3 [13, 52].

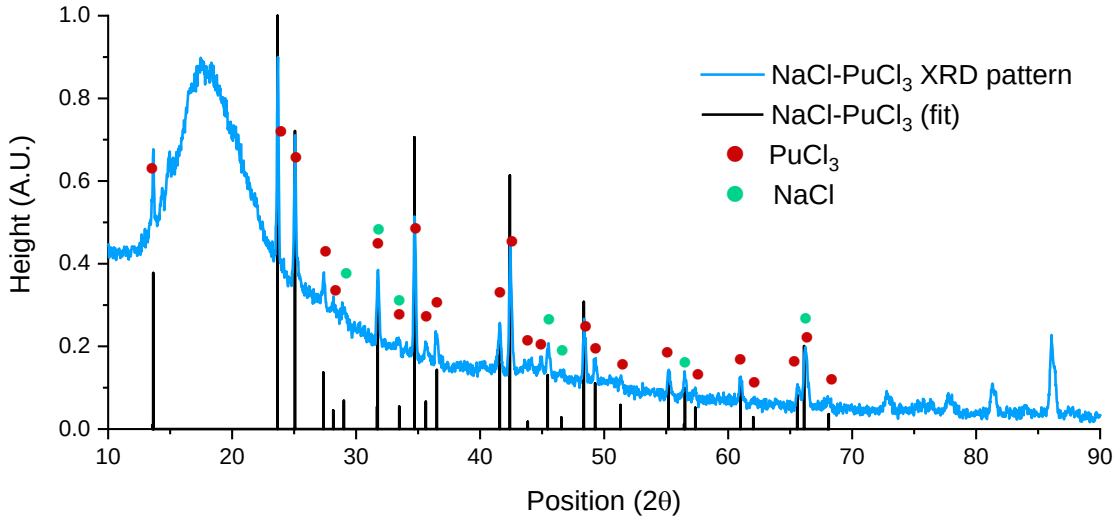

Figure 5. XRD pattern for eutectic NaCl-$PuCl_3$.

3.2 Salt Stability, Melting Temperature, and Enthalpy

Prior to melting temperature and other property measurements the stability of the salt at elevated temperatures was investigated on the STA by monitoring the mass change as a function of temperature. Each heating rate used a new sample. Results for mass change as a function of heating rate and time are provided in Figure 6. The sample with the fastest heating rate was exposed to the highest temperature. No clear trend with heating and cooling was observed for the sample as is evident by the lack of "stairstep" in the mass change curves. The overall sample mass change was observed to be $< \pm 0.25\%$ for all samples.

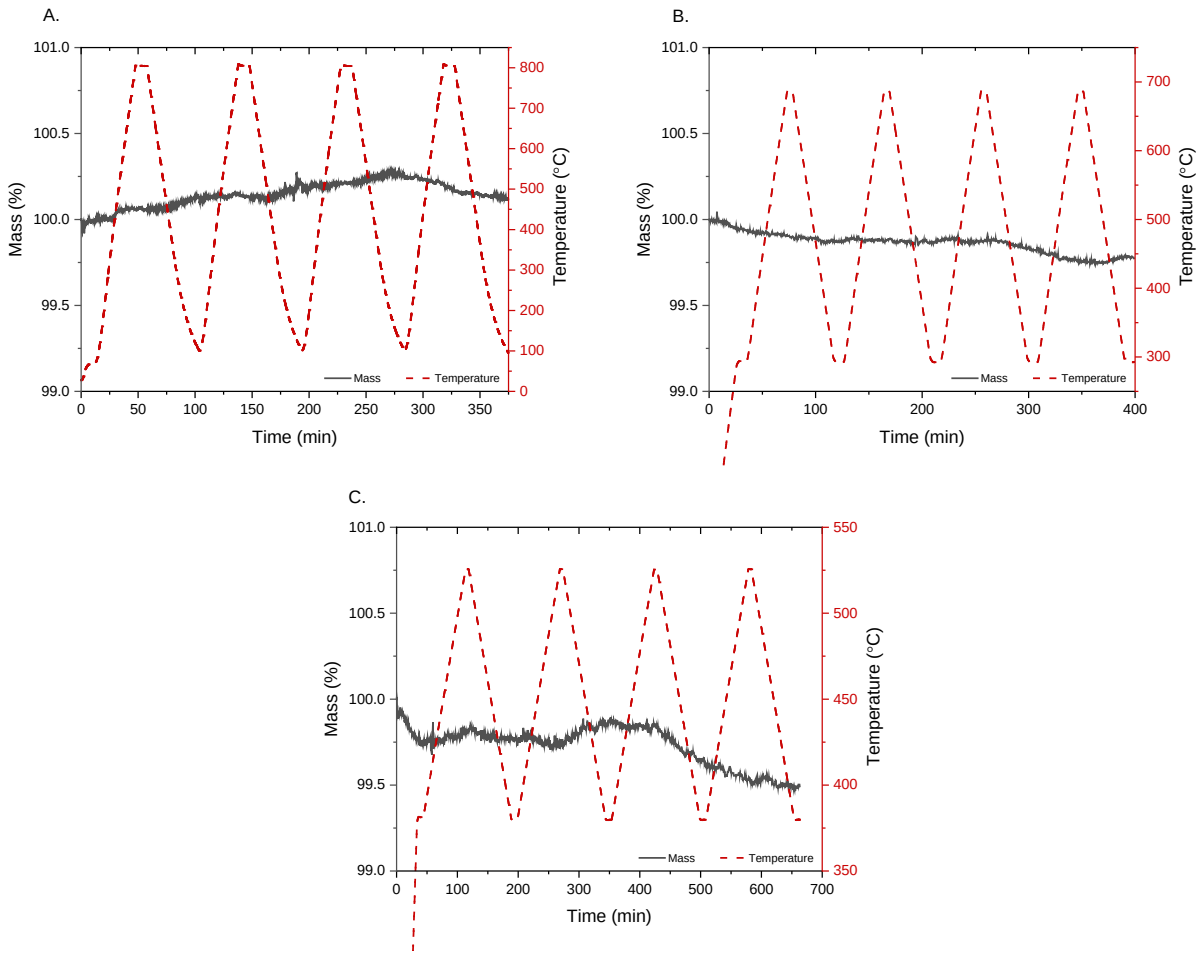

Figure 6. Mass changed curves as a function of time and temperature for the NaCl-$PuCl_3$ ingot: A. 20°C/min, B. 10°C/min, and C. 2°C/min.

The melting point was investigated using three separate samples, each experiencing a different heating rate: 20, 10, and 2°C/min. Each sample was subjected to four heating and cooling cycles, the first was discarded while inflections from the other three were averaged and used to report temperature dependent transitions. The second heating thermogram for each heating rate is shown in Figure 7A during heating and Figure 7B for cooling. Upon heating, only one peak was observed, attributed to the solid to liquid transition at the eutectic temperature. The eutectic onset temperature is 451°C, while the peak and end temperature are 455 and 456°C, determined using linear regression from the average values determined at each heating rate. The eutectic temperature, 451°C, determined in this work closely matches other reported eutectic temperatures of 453°C [15] and 450°C [50].

As labeled in Figure 7B, there are two distinct peaks upon cooling where peak 1 occurs at various temperatures and is attributed to recrystallization of the eutectic NaCl-$PuCl_3$ mixture. Peak 2 occurs at approximately 455°C, and while the cause of this peak is unclear, it could be due to cooling kinetics within the sample crucible. Referring to the elemental and isotopic analysis of the ingot material, no metal impurities were detected, and the concentration of $PuCl_3$ was determined to be 36.6 mol%. Analysis of the 2°C/min heating peak shows the eutectic transition peak has a width of 10°C, occurring between 450–460°C. Although there is only one peak shown experimentally to occur in this temperature range, if the salt differs very slightly from the eutectic composition, then a small peak may be hidden within the larger eutectic transition peak. Referencing the NaCl-$PuCl_3$ phase diagram developed by Bjorklund et al. [15]

indicates that a 10°C increase in temperature at most could be the result of a salt having a $PuCl_3$ composition between 35.47–37.52 mol%. Although it is not recommended to use temperatures from cooling curves when analyzing molten salts, due to supercooling effects, a solidus temperature at 455°C would indicate a $PuCl_3$ composition of 36.8 mol%, which is 0.5 mol% higher than analytical results indicate. It can therefore be concluded from analytical results as well as analysis of the solidus and liquidus temperature that the NaCl-$PuCl_3$ used in this study has a $PuCl_3$ concentration between 36.3 to 36.8 mol%.

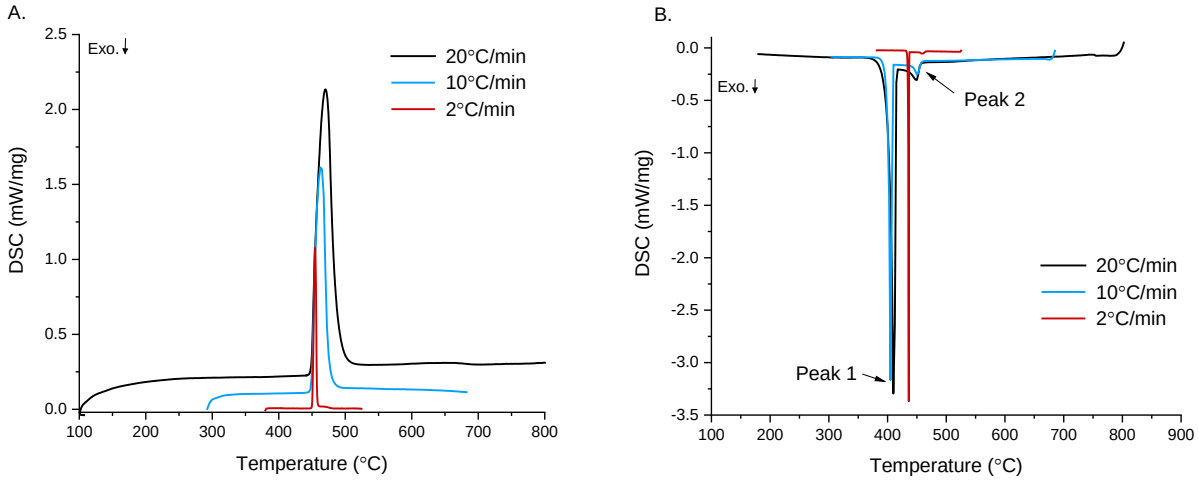

Figure 7. Thermograms for three sample each analyzed at a different heating rate. A. heating curves; B. cooling curves.

The enthalpy of fusion, ΔH_f^o, for the NaCl-$PuCl_3$ ingot was determined by integrating the area under the eutectic peak transition, where ΔH_f^o ranged from 134.8 to 148.4 J/g with an average for all three heating rates of 140.7 ± 8.4 J/g. The enthalpy of crystallization, ΔH_C^o, was determined to be -130.9 ± 11.4 J/g.

The eutectic and liquidus temperature of 25 mol% $PuCl_3$ in NaCl was determined to be 450 and 599°C, respectively. These values were determined following the experimental approach described for the eutectic composition, where three heating rates were used to determine the onset eutectic temperature and liquidus temperature. The enthalpy of fusion for the 25 mol% $PuCl_3$ in NaCl was determined to be 171.4 ± 11.4 J/g.

3.3 Heat Capacity

Three individual liquid state heat capacity measurements were performed using a new sample for each group of measurements, and in total, three samples were analyzed. Before heat capacity measurements, heat flow calibrations were verified using the sapphire calibration standard on each sample. If the experimentally determined sapphire heat capacity deviated from standard values [53] by > 5%, the sapphire heat capacity was deemed inadequate, and it was performed again. Heat capacity was determined following standard test methods [33]. An example of sapphire heat capacity measurement is shown in Figure 8A.

For NaCl-$PuCl_3$ eutectic samples, the experimental heat capacities for all samples are shown in Figure 8B where the heat capacity was done in triplicate for each sample. The reported heat capacity was determined by taking the average values for all heat capacity as shown in Figure 8C with error bars representing one standard deviation. Experimentally determined heat capacity was shown to vary slightly with temperature between 0.67 to 0.57 J/g·K, with an average value of 0.637 ± 0.03 J/g·K (104 ± 5 J/mol·K) within the range of temperatures from 500 to 720°C, as shown in Figure 8C.

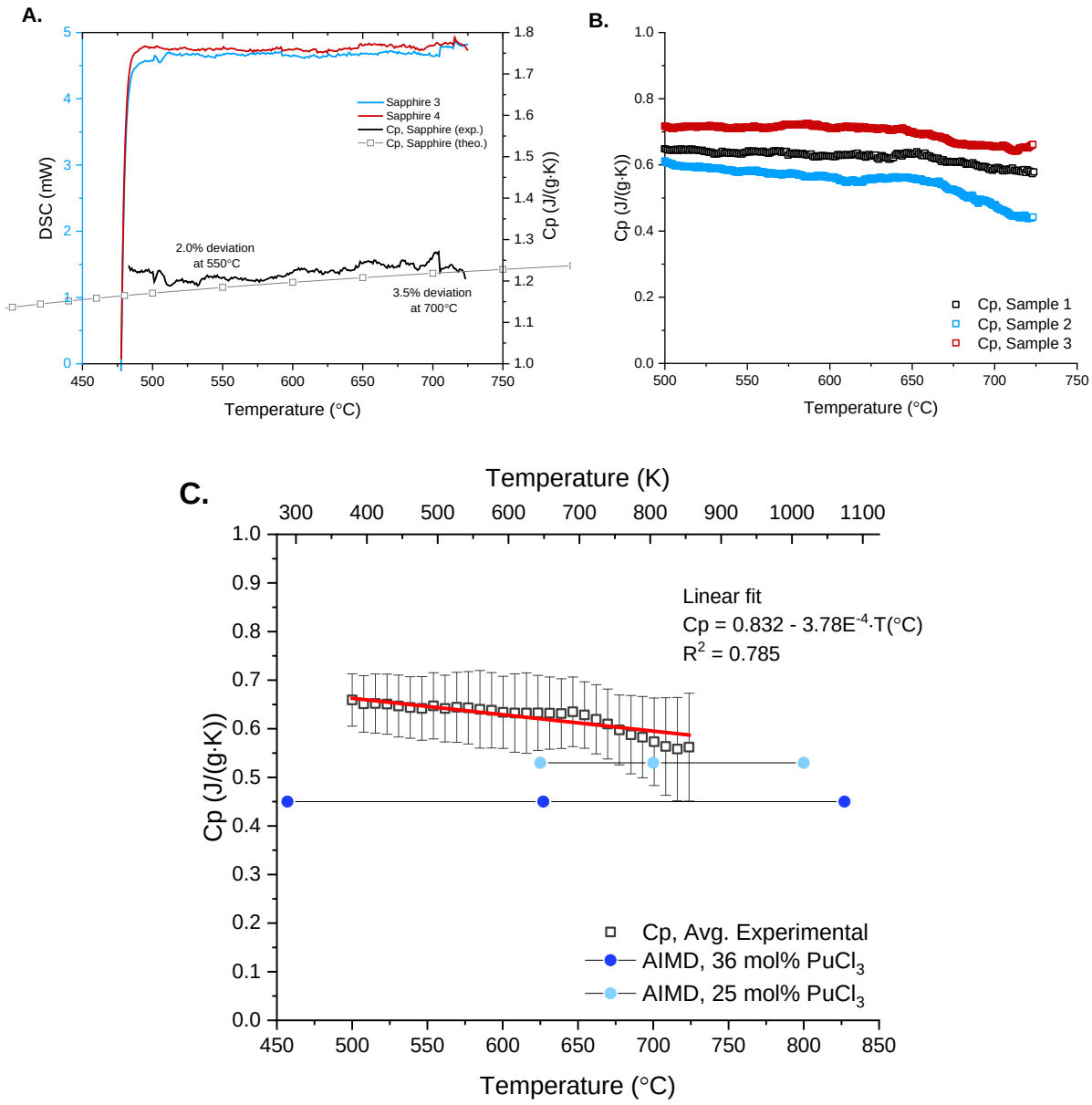

Figure 8. Summary of heat capacity. A. DSC curves for sapphire standard comparing experimentally determined and NIST reported sapphire heat capacity. B. Experimental heat capacity values for three NaCl-$PuCl_3$ eutectic samples. C. Averaged heat capacity valued with error bars of one standard deviation derived from experimental Cp measurements along with AIMD values calculated for two compositions.

The specific heat was calculated from AIMD simulations using Equation 5, where H is the total energy, V is the volume, and P is the pressure of the during NPT simulations, δT is a temperature change, and the notation < > indicates the ensemble average values. Ideally, δT should be small enough to reduce the numerical error. However, we found that $\langle H + VP \rangle_{NPT}$ is linear with temperature as seen in Figure 8C; therefore, we can use the slope of the line over the range to simulate temperatures to estimate heat capacity.

$$C_p = \frac{\delta \langle H+VP \rangle_{NPT}}{\delta T} \qquad \text{Equation 5}$$

Experimentally determined heat capacity values were higher than the respective computational values for the eutectic mixture. For pure $PuCl_3$, the calculated specific heat capacity has been reported to be 0.293 J/g·K (101.2 J/mol·K) [54] while the specific heat capacity for NaCl is known to be 50.3 J/mol·K (0.856 J/g·K). An estimated heat capacity, based on the molar ratio and assuming the molecular weight for Pu-239 trichloride, is calculated to be 68.4 J/mol·K (0.419 J/g·K). The estimated heat capacity value is slightly lower than the AIMD-derived value of 0.45 J/mol·K as well as the experimentally determined value.

The Pu-metal starting material is not isotopically pure Pu-239 as shown in Table 5 which may alter the experimental heat capacity slightly. Studies to determine the energy produced by alpha disintegrations in a pure Pu-239 source found that the total energy produced per alpha-disintegration in Pu-239 is 5.23 MeV ($8.38 \cdot 10^{-6}$ erg/atom) [55]. In addition, a study to determine the heat capacity of PuC synthesized from a 99.93% Pu-metal found that the sample exhibited "self-heating" due to alpha disintegrations and enthalpy values had to be corrected to account for heat generated within the sample [56]. The experimental heat capacity data in Figure 8C are uncorrected for internal heating sources, and this may lead to the differing values between the experiment and calculations.

This work highlights an important point, in that, for salts containing radioactive substances, such as fuel salts where the sample can exhibit self-heating, heat capacity values may vary from theoretical calculations and will vary experimentally depending on the isotopic composition. Deviation between AIMD and experimentally determined values may also arise if the enthalpy of mixing predicted by simulations does not accurately predict the modeled system; variation in modeled enthalpy is evident in literature [49, 50, 57].

3.4 Density

The density of the molten NaCl-$PuCl_3$ mixtures was studied by measuring the buoyancy of a nickel bobber (99.999%) in the liquid salts at temperatures between 500–800°C. The experimentally determined values of density for each temperature profile and composition are shown in Figure 9; it is apparent that the effects of the heating/cooling schedule are non-existent. Figure 9 shows the combined results and linear equation of fit, representing the equation for density as a function of temperature. Independent experiment trials determined the 36 mol% and 25 mol% $PuCl_3$ in NaCl salt to have liquid state densities as outlined in Equations 6 and 7, respectively.

$$\rho_{36mol\%\ PuCl_3} = 3.8589 - 9.5324 \cdot 10^{-4}(T, °C) \qquad R^2 = 0.9795 \qquad \text{Equation 6}$$

$$\rho_{25mol\%\ PuCl_3} = 3.3945 - 8.4546 \cdot 10^{-4}(T, °C) \qquad R^2 = 0.9912 \qquad \text{Equation 7}$$

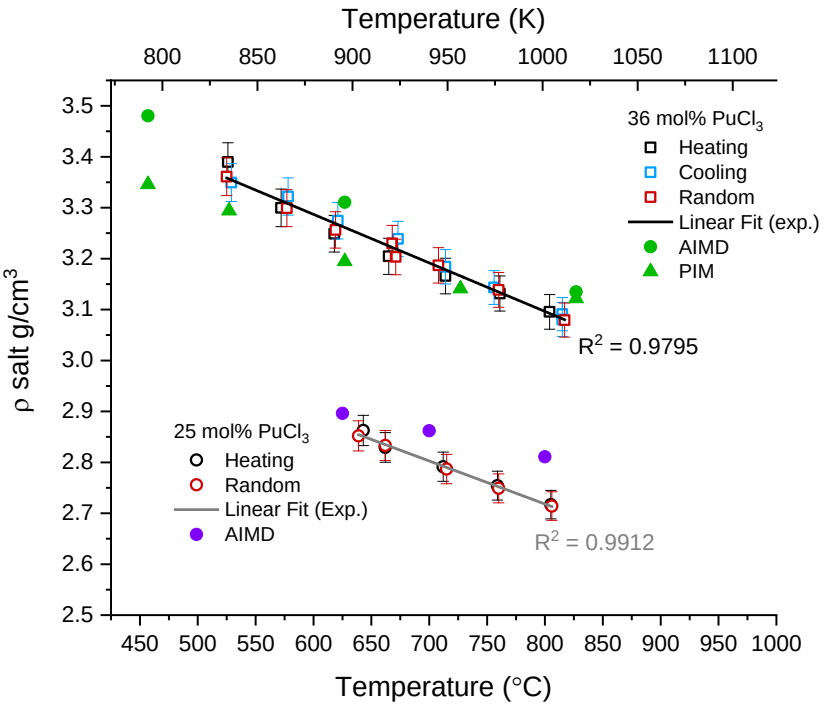

Figure 9. Experimental and calculated density values for 36 mol% and 25 mol% $PuCl_3$ in NaCl carrier salt.

Figure 9 shows the density determined by using CMD and AIMD approaches with experimental data. Predicting the density of actinide molten-salt systems, especially with actinide-rich composition, is a challenging task due to high computing cost associated with electronic structure calculations of the system. Given how close the CMD and AIMD values are, CMD should provide a good starting configuration for AIMD. For the eutectic composition, the PIM density appeared to be lower than the AIMD density at a wide range of temperature; nonetheless, they are very consistent with experimental data. Both computational and experimental results show a linear dependence of the density on the temperature: $\rho = \rho_0 - A \times T$. The temperature-density correlation coefficient from AIMD and experiment is 9.3×10^{-4} and 9.5×10^{-4} (g/cm^3·K), respectively. The same approach was used to determine the density for 25 mol% $PuCl_3$ systems.

4. CONCLUSION

A non-traditional, gas:solid, synthesis path using NH_4Cl for chlorinating Pu-metal to obtain $PuCl_3$ salts was demonstrated. NaCl was added to the reaction to form the eutectic composition, 64 mol% NaCl - 36 mol% $PuCl_3$, and was determined to have a purity of 99.7% with trace amounts of iron, americium, and uranium. By adding NaCl to the eutectic salt, 25 mol% $PuCl_3$ (in NaCl) was made. Both salt compositions were shown to be stable up to 800°C, and their melting points and enthalpies of fusion were measured with high repeatability. The melting point of the 36 mol% $PuCl_3$ was determined to be 451°C while the melting point of 25 mol% $PuCl_3$ was determined to be 598°C. Enthalpy of these salt systems had not been experimentally determined previously; however, this work determined the enthalpy of fusion for the 36 mol%$PuCl_3$ and 25 mol% $PuCl_3$ to be 140.7 ± 8.4 J/g and 171.4 ± 11.4 J/g, respectively.

The heat capacity of the salt was measured and reinforced the idea that for studying thermal properties of radioactive salts, the self-heating due to alpha disintegrations may need to be considered to explain discrepancies in measured properties containing different ratios of isotopes and therefore decay products. The experimentally determined heat capacity was shown to be slightly higher than AIMD

simulation values. However, both experimental and calculated values showed little dependance on temperature within the range measured. For the eutectic salt, heat capacity was determined experimentally to be 0.637 ± 0.030 J/g·K between 500 to 720°C while AIMD simulations determined a Cp of 0.45 J/g·K over the same temperature range. These discrepancies are expected given the experimental challenges of measuring heat capacity. From the theory point of view, constant pressure molecular simulations are also extremely sensitive and require extensive molecular models and sampling. Overall, this work shows that modeling captures the essential trends in these systems and can be used to supplement experimental data.

A combination of experimental measurements and molecular dynamics simulations were used to determine the density of the two salt compositions. Experimental densities, in the liquid state, were shown to have a linear decrease with temperature. As expected, the density of the 36 mol% $PuCl_3$ mixture was higher than that of the 25 mol% $PuCl_3$ salt. Experimental and AIMD values for density of the eutectic salt system were in good agreement and of similar slope; while computed density values for the 25 mol% $PuCl_3$ salt showed a differing slope, values were also in close agreement with experimental.

The data reported in this work are both experimental and computation values. Some of the data presented here are the only known data available for these salt systems in literature. Further work is needed to verify accuracy and reduce errors, but this serves as a key baseline study for the otherwise unknown NaCl-$PuCl_3$ binary salt system.

5. REFERENCES

1. Taube, M. and J. Ligou. 1974. “Molten plutonium chlorides fast breeder reactor cooled by molten uranium chloride.” *Annals of Nuclear Science and Engineering* 1 (4): 277–281. https://doi.org/10.1016/0302-2927(74)90045-2.
2. Nelson, P. A. D. K. Butler, M. G. Chasanov, and D. Meneghetti. 1967. “Fuel Properties and Nuclear Performance of Fast Reactors Fueled with Molten Chlorides.” *Nuclear Applications* 3 (9): 540–547. https://doi.org/10.13182/NT67-A27935.
3. Chasanov, M. G. 1965. “Fission-Product Effects in Molten Chloride Fast-Reactor Fuels.” *Nuclear Science and Engineering* 23 (2): 189–190. https://doi.org/10.13182/NSE65-A28145.
4. International Atomic Energy Agency. 2021. “The Potential Role of Nuclear Energy in National Climate Change Mitigation Strategies.” IAEA-TECDOC-1984, IAEA.
5. Faure, B. and T. Kooyman. 2022. “A comparison of actinide halides for use in molten salt reactor fuels.” *Progress in Nuclear Energy* 144: 104082. https://doi.org/10.1016/j.pnucene.2021.104082.
6. Snyder, C., M. H. West, M. D. Ferran, and K. W. Fife. 1988. “The chlorination of plutonium dioxide.” United States, 18.
7. Tolley, W. B. 1953. “Plutonium Trichloride: Preparation By Reaction With Phosgene or Carbon Tetrachloride, and Bomb Reduction to Metal.” United States. https://doi.org/10.2172/4198998.
8. Stroud, M. A., R. R. Salazar, K. D. Abney, E. A. Bluhm, and J. A. Danis. 2006. “Purification of Plutonium Chloride Solutions via Precipitation and Washing.” *Separation Science and Technology* 41 (10): 2031–2046. https://doi.org/10.1080/01496390600742997.
9. Boreham, D., J. H. Freeman, E. W. Hooper, I. L. Jenkins, and J. L. Woodhead. 1960. “The preparation of anhydrous plutonium trichloride.” *Journal of Inorganic and Nuclear Chemistry* 16 (1): 154–156. https://doi.org/10.1016/0022-1902(60)80102-9.
10. Garner, C. S. 1944. “The Preparation of Plutonium Trichloride.” Los Alamos National Laboratory. https://permalink.lanl.gov/object/tr?what=info:lanl-repo/lareport/LA-00112.
11. Paget, T., J. Mcneese, K. Fife, M. Jackson, and R. Watson. “Chapter 6: Molten Salt Chemistry of Plutonium.” in *Plutonium Handbook* (La Grange Park: American Nuclear Society, 2018).
12. Johnson, K. W. R. and J. A. Leary. 1964. “The Pu-PuCl3 system.” *Journal of Inorganic and Nuclear Chemistry* 26 (1): 103–105. https://doi.org/10.1016/0022-1902(64)80236-0.
13. Herrmann, S. D., H. Zhao, K. K. Bawane, L. He, K. R. Tolman, and X. Pu. 2022. “Synthesis and characterization of uranium trichloride in alkali-metal chloride media.” *Journal of Nuclear Materials* 565, 153728. https://doi.org/10.1016/j.jnucmat.2022.153728.
14. Voronenkov, V., et al. 2020. “Hydride Vapor-Phase Epitaxy Reactor for Bulk GaN Growth.” *2019 Compound Semiconductor Week* 217 (3): 1900629. https://doi.org/10.1109/ICIPRM.2019.8819335.
15. Bjorklund, C. W., J. G. Reavis, J. A. Leary, and K. A. Walsh. 1959. “Phase Equilibria in the Binary Systems PuCl3–NaCl and PuCl3–LiCl.” *The Journal of Physical Chemistry* 63 (10): 1774–1777. https://doi.org/10.1021/j150580a049.
16. Outotec. 2019. “HSC Chemistry 9.” Metso Outotec Finland Oy.
17. Feldman, S. R. 2011. “Sodium Chloride.” *in Kirk-Othmer Encyclopedia of Chemical Technology*. 1-27. https://doi.org/10.1002/0471238961.1915040902051820.a01.pub3.
18. Beard, C., et al. 2008. “Actinide Research Quarterly, in Plutonium Processing at Los Alamos.” ed. M. Coonley. Los Alamos National Laboratory: Stockpile Manufacturing and Support (SMS) Directorate. p. 20.
19. Phipps, T. E., G. W. Sears, R. L. Seifert, and O. C. Simpson. 1950. “The Vapor Pressure of Plutonium Halides.” *The Journal of Chemical Physics* 18 (5): 713–723. https://doi.org/10.1063/1.1747733.

20. Robinson, H.P. 1949. “Determination of the Melting Points of Plutonium (III) Chloride and Plutonium (III) Bromide.” *The Transuranium Elements*. 952–956.
21. Konings, R. J. M., L. R. Morss, and J. Fuger. “The Chemistry of the Actinide and Transactinide Elements Thermodynamic Properties of Actinides and Actinide Compounds.” ed. L. R. Morss, N. M. Edelstein, and J. Fuger. Vol. 4. The Netherlands: Springer. 2113–2224. https://doi.org/10.1007/1-4020-3598-5_19.
22. Burns, J. H., J. R. Peterson, and J. N. Stevenson. 1975. “Crystallographic studies of some transuranic trihalides: $^{239}PuCl_3$, $^{244}CmBr_3$, $^{249}BkBr_3$ and $^{249}CfBr_3$.” *Journal of Inorganic and Nuclear Chemistry*. 37 (3): 743–749. https://doi.org/10.1016/0022-1902(75)80532-X.
23. Maenpaa, L. and A. Roine. HSC Chemistry 9, in H, S, and Cp Database. 2019, Outotec Research Center.
24. Lemire, R. J., et al. 2001. “Chemical Thermodynamics of Neptunium and Plutonium.” *Chemical Thermodynamics* 4, ed. O.N.E. Agency. North Holland Elsevier Science.
25. Cleveland, J. M. 1980. “Plutonium Handbook: A Guide to the Technology.” *Compounds of Plutonium*, ed. O. J. Wick. Vol. 1. La Grange Park, IL: The American Nuclear Society.
26. Richmond, S., et al. 2010. “The solubility of hydrogen and deuterium in alloyed, unalloyed and impure plutonium metal.” *IOP Conference Series: Materials Science and Engineering*, 9: 012036.
27. Haschke, J.M., T.H. Allen, L. A. Morales. 2000. “Surface and Corrosion Chemistry of Plutonium.” *Los Alamos Science* 26: 252–273.
28. Bradley, D. 1957. “The Preparation and Properties of the Chlorides of Uranium, Plutonium, Thorium and of the Fission Product Chlorides, A.E.R.” *United Kingdom Atomic Energy Authority Research Group*.
29. Meier, R., et al. 2012. “Recycling of Uranium from Uranium-Aluminum alloys by Chlorination with HCl(g).” *Procedia Chemistry* 7: 785–790. https://doi.org/10.1016/j.proche.2012.10.119.
30. Sonneveld, E. J. and J. W. Visser. 1975 “Automatic collection of powder data from photographs.” *Journal of Applied Crystallography* 8 (1): 1–7.
31. American Society for Testing and Materials. 2018. “Standard Test Method for Temperature Calibration of Differential Scanning Calorimeters and Differential Thermal Analyzers.” ASTM E967-18, ASTM International.
32. American Society for Testing and Materials. 2018. “Standard Test Method for Thermal Lag of Thermal Analysis Apparatus.” ASTM E3142-18a, ASTM International.
33. American Society for Testing and Materials. 2018. “Standard Test Method for Determining Specific Heat Capacity by Differential Scanning Calorimetry.” ASTM E1269-11, ASTM International.
34. Duemmler, K., et al. 2022. “Evaluation of thermophysical properties of the LiCl-KCl system via *ab initio* and experimental methods.” *Journal of Nuclear Materials* 559. https://doi.org/10.1016/j.jnucmat.2021.153414.
35. Hidnert, P. 1957. “Thermal Expansion of Some Nickel Alloys.” *Journal of Research of the National Bureau of Standards* 58 (2): 89–92.
36. VandeVondele, J., et al. 2005. “QUICKSTEP: Fast and accurate density functional calculations using a mixed Gaussian and plane waves approach.” *Computer Physics Communications* 167 (2): 103–128. https://doi.org/10.1016/j.cpc.2004.12.014.
37. Kühne, T. D., et al. 2020. “CP2K: An electronic structure and molecular dynamics software package - Quickstep: Efficient and accurate electronic structure calculations.” *The Journal of Chemical Physics* 152 (19): 194103. https://doi.org/10.1063/5.0007045.
38. Salanne, M. and P. A. Madden. 2011. “Polarization effects in ionic solids and melts.” *Molecular Physics* 109 (19): 2299–2315. https://doi.org/10.1080/00268976.2011.617523.

39. Parrinello, M. and A. Rahman. 1981. “Polymorphic transitions in single crystals: A new molecular dynamics method.” *Journal of Applied Physics* 52 (12): 7182–7190. https://doi.org/10.1063/1.328693.
40. Martyna, G.J., M.L. Klein, and M. Tuckerman. 1992. “Nosé–Hoover chains: The canonical ensemble via continuous dynamics.” *The Journal of Chemical Physics* 97 (4): 2635–2643. https://doi.org/10.1063/1.463940.
41. Perdew, J. P., K. Burke, and M. Ernzerhof. 1996. “Generalized gradient approximation made simple.” *Physical Review Letters* 77 (18): 3865–3868. https://doi.org/10.1103/PhysRevLett.78.1396.
42. Grimme, S., et al. 2010. “A consistent and accurate *ab initio* parametrization of density functional dispersion correction (DFT-D) for the 94 elements H-Pu.” The Journal of Chemical Physics 132 (15): 154104. https://doi.org/10.1063/1.3382344.
43. Goedecker, S., M. Teter, and J. Hutter. 1996. “Separable dual-space Gaussian pseudopotentials.” *Physical Review B* 54 (3): 1703–1710. https://doi.org/10.1103/PhysRevB.54.1703.
44. Lu, J.-B., et al. 2021. “Norm-Conserving Pseudopotentials and Basis Sets to Explore Actinide Chemistry in Complex Environments.” *Journal of Chemical Theory and Computation* 17 (6): 3360–3371. https://doi.org/10.1021/acs.jctc.1c00026.
45. VandeVondele, J. and J. Hutter. 2007. “Gaussian basis sets for accurate calculations on molecular systems in gas and condensed phases.” *Journal of Chemical Physics* 127 (11). https://doi.org/10.1063/1.2770708.
46. Lu, J. B., et al. 2019. “Norm-Conserving Pseudopotentials and Basis Sets To Explore Lanthanide Chemistry in Complex Environments.” *Journal of Chemical Theory and Computation* 15 (11): 5987–5997. https://doi.org/10.1021/acs.jctc.9b00553.
47. Lippert, G., J. Hutter, and M. Parrinello. 1997. “A hybrid Gaussian and plane wave density functional scheme.” *Molecular Physics* 92 (3): 477–487. https://doi.org/10.1080/002689797170220.
48. Clow, J., et al. 1994. “Specific activities and DOE-STD-1027-92 hazard Category 2 thresholds, LANL fact sheet.” LA-12846-MS, Los Alamos National Laboratory. https://doi.org/10.2172/10190930.
49. Beneš, O. and R. J. M. Konings. 2008. “Thermodynamic evaluation of the NaCl–MgCl2–UCl3–PuCl3 system.” *Journal of Nuclear Materials* 375 (2): 202–208. https://doi.org/10.1016/j.jnucmat.2008.01.007.
50. Yin, H., et al. 2020. “Thermodynamic description of the constitutive binaries of the NaCl-KCl-UCl3-PuCl3 system.” Calphad 70. https://doi.org/10.1016/j.calphad.2020.101783.
51. Zachariasen, W. 1948. “Crystal chemical studies of the 5f-series of elements. I. New structure types.” *Acta Crystallographica* 1 (5): 265–268. https://doi.org/10.1107/S0365110X48000703.
52. Zachariasen, W. H. and F. H. Ellinger. 1959. “Unit cell and thermal expansion of β-plutonium metal.” *Acta Crystallographica* 12 (3): 175–176. https://doi.org/10.1107/S0365110X59000524.
53. Archer, D. G. 1993. “Thermodynamic Properties of Synthetic Sapphire (α-Al2O3), Standard Reference Material 720 and the Effect of Temperature-Scale Differences on Thermodynamic Properties.” *Journal of Physical and Chemical Reference Data* 22 (6): 1441–1453. https://doi.org/10.1063/1.555931.
54. Guillaumont, R., et al. 2003. “Update on the Chemical Thermodynamics of Uranium, Neptunium, Plutonium, Americium and Technetium.” Vol. 5. OECD Nuclear Energy Agency.
55. Stout, J. W. and W. M. Jones. 1947. “A Calorimetric Determination of the Energy Produced by Plutonium (239).” *Physical Review* 71 (9): 582–585. https://doi.org/10.1103/PhysRev.71.582.

56. Kruger, O. L. and H. Savage. 1964. “Heat Capacity of Plutonium Monocarbide from 400° to 1300°K.” *The Journal of Chemical Physics* 40 (11): 3324–3328. https://doi.org/10.1063/1.1725001.
57. Schorne-Pinto, J., et al. 2022. “Correlational Approach to Predict the Enthalpy of Mixing for Chloride Melt Systems.” *ACS Omega* 7 (1): 362–371. https://doi.org/10.1021/acsomega.1c04755.